Dynamical evolution of asteroid fragments originating near the ν_6 resonance

Takashi Ito and Renu Malhotra

Lunar & Planetary Laboratory, The University of Arizona, Tucson, AZ 85721–0092, USA

Correspondence author's e–mail: tito@LPL.arizona.edu

Number of pages: 34
Number of tables: 1
Number of figures: 11

Proposed running head: Dynamical evolution of asteroid fragments

Editorial correspondence to:

Takashi Ito Lunar & Planetary Laboratory
The University of Arizona
Tucson, AZ 85721–0092
TEL: (520) 621–2883
FAX: (520) 621–4933
E-mail: tito@LPL.arizona.edu

Abstract

We performed numerical integrations of test particles in the vicinity of the ν_6 resonance in the main asteroid belt. The purpose of our integrations is to explore the dynamical evolution of asteroid fragments from a hypothetical asteroid disruption event near the ν_6 resonance. Compared with previous studies, we simulate an order of magnitude larger number of particles, and we include the effects of eight planets from Mercury to Neptune. We follow the particles for up to 100 million years and up to 100 AU heliocentric distance. Our main results are: (i) collisional probability of asteroid fragments on the planets is generally low (4–5% for Venus and Earth, and less than 1% for Mercury and Mars) whereas the collision probability for the Sun is large (50–70% or higher), and (ii) decay timescale of the particle population is typically 10–20 million years, but can be much longer, depending on the location of disruption. We find that the effects of ν_6, close encounters with planets, and the Kozai mechanism all play important roles in the orbital history of asteroid fragments that enter the terrestrial planetary region. The particles that survive 100 million years or longer typically owe their long dynamical lifetime to the Kozai mechanism, and tend to have higher inclinations. Our results also suggest that 10–15% of asteroid fragments reach heliocentric distance > 100 AU, and may survive in the Oort cloud.

Keywords: Asteroids, Dynamics; Resonances, Terrestrial planets

1. Introduction

Our solar system planets have evolved through a large number of collisions. The impact history of the Earth and of the other terrestrial planets is still partially evident in the numerous craters on their surfaces. Although there are several hypotheses on the source of the projectiles that created the impact craters on the terrestrial planets, the main belt asteroids have been considered the most plausible one. The main belt asteroids are also regarded as a primary source of most meteorites and majority of the near-Earth asteroids (NEAs) or the near-Earth objects (NEOs). Pioneering works by Wetherill (1979), Wisdom (1983) and Wetherill (1985) showed the orbital resonances with Jupiter in the main asteroid belt can force asteroids to cross the orbits of the terrestrial planets. Later, Wetherill (1985, 1987, 1988) developed analytical approximations for the resonant effect of the ν_6 and the 3:1 resonances along with an Öpik–Arnold Monte Carlo orbital evolution model. His research indicated that the NEAs are supplied by disruption or collisional events that occur in the vicinity of some resonances in the main asteroid belt. Resonant dynamics pushes asteroid fragments into terrestrial planetary orbits on timescale of million years or more.

Our understanding of the mechanisms that transport objects from the main belt to the Earth has progressed rapidly in recent years due to important advances in three areas: analytical modeling of resonant dynamics, effective numerical algorithms, and availability of fast and inexpensive computer hardware. Some analytical theories indicate that many secular and mean motion resonances can be responsible for transporting asteroids to Mars-crossing and Earth-crossing orbits (Froeschlé and Morbidelli, 1994; Morbidelli and Nesvorný, 1999). The timescale of such resonant dynamics is relatively short, and the orbits of the asteroids in resonances quickly become sun-grazing or Jupiter-crossing (Farinella et al., 1994; Levison and Duncan, 1994; Froeschlé et al., 1995).

Along this line, Gladman et al. (1997) performed numerical simulations of hundreds of test particles placed in orbital resonances in the main asteroid belt. They showed that the typical dynamical lifetime of objects that could become NEAs is only a few million years, while the majority of them are removed from the inner solar system by being transferred to Jupiter-crossing orbits or by colliding with the Sun. This work was extended by Morbidelli and Gladman (1998) who performed numerical integrations of about 2000 particles originally placed in the ν_6, 3:1, and 5:2 resonances in the main belt. They examined the orbital evolution of the asteroids, and compared the results with the observational data of meteorites that hit the Earth. In the same year, Zappalà et al. (1998) evaluated the number of impactors produced in different size ranges by disruption events that might have created some existing asteroid families. Their estimate shows that an impact flux could last 2–30 million years in the form of asteroid showers, which could be responsible for the lunar cataclysm. More recently, Bottke et al. (2002a) created a model NEO population that was fit to known NEOs. They performed numerical integrations of thousands of test particles initially placed in several possible source regions of NEOs (most of them are in the main asteroid belt). Their numerical result was used to construct time-dependent probability distributions in orbital element space.

These recent studies have greatly overcome the shortcomings of the older studies which used Öpik–Arnold type geometrical and kinematic models. However, even with the modern numerical

orbit integration techniques, computer resource limitations still make it necessary to make simplifying assumptions, to use simplified dynamical models, and to limit simulations to a relatively small number of particles. For example, the total number of particles that the recent studies have used is a few hundreds to a few thousands; this is insufficient for a statistical discussion of the collision probability of asteroids on planets. An example of a simplification of the dynamical models is that most studies have not included Mercury, considering only the seven planets from Venus to Neptune. Also, no study thus far has included the orbital mechanics of the Earth–Moon system when estimating the collisional probability of NEAs on the Earth or on the Moon. These issues might seem negligible in the conventional context of the orbital distribution of NEAs. However, as we move closer towards the goal of accurately calculating the collisional frequency and collision probability of asteroids on the terrestrial planets with a large number of particles, and eventually comparing the dynamical model results with the geological crater record, we should like to assess the significance of the effects that have been neglected in previous studies.

In this paper, we study in detail the orbital motion of more than 14,000 asteroid fragments that come from the vicinity of the ν_6 secular resonance after a hypothetical disruption event in the main belt. Our purpose here is to examine their orbital evolution and to estimate the collision probability on the terrestrial planets. We describe our dynamical model and numerical method in Section 2. Section 3 is devoted to our numerical results in detail: decay rate, production rate of near-Earth objects, collision sequence on the terrestrial planets, and some other dynamical characteristics of the asteroid fragments. Based on the numerical results so far obtained, we discuss some implications on the real dynamical evolution of asteroid fragments in our solar system in Section 4. Our conclusions are summarized in Section 5.

2. Dynamical model and initial conditions

To trace the orbital evolution of asteroid fragments created by a disruption event, we start with test particles near the ν_6 resonance and numerically integrate their orbital evolution under the gravitational effect of eight major planets, Mercury to Neptune. The major planets are assumed to have their present masses and orbital elements. All celestial bodies are treated as point masses dynamically, although planetary and solar physical radii matter when we calculate collisions between test particles and large bodies. No consideration is given to post-Newtonian gravity, tidal forces, gas drag, solar equatorial bulge, and non-gravitational or dissipative effects such as the Yarkovsky effect.

To emulate a disruption event that is supposed to have created a swarm of asteroid fragments, we make two assumptions. First, we assume an isotropic disruption; i.e. the initial velocity vector of asteroid fragments with respect to the initial position of the parent body is isotropically distributed in three-dimensional space, generated by random numbers (we discuss more about the validity of this assumption in Section 4). Second, we consider an equal-velocity disruption; all fragments have the same initial ejection velocity, v_0. We chose $v_0 = 0.1$ or 0.2 km/s, and we also tested $v_0 = 0.8$ km/s for comparison. For the currently existing asteroid families, estimates of the initial ejection velocity of asteroid fragments are in the range of $v_0 = 0.1$–0.2 km/s

(Zappalà et al., 1996; Cellino et al., 1999). Our assumption of $v_0 = 0.1$–0.2 km/s is based on this estimate. We discuss this assumption in Section 4.

We selected seven initial disruption locations to sample a range of locations in the vicinity of the ν_6 resonance in orbital element space (semimajor axis a, eccentricity e, inclination I), and we adopted a physically reasonable relationship of $e = 2I$. The detailed initial conditions of the disruption location of the test particles in our numerical integrations are shown in Fig. 1 and the upper part of Table 1. The initial values of the angle variables for disruption center, such as mean anomaly l, longitudes of ascending node Ω, and argument of perihelion ω, are randomly selected from 0 to 2π. Fig. 1

For each of the seven initial disruption locations, we placed 1000–3000 test particles (14033 particles in total), and numerically integrated their orbital evolution for up to 100 million years. When a test particle goes within the present physical radius of the Sun or that of planets, we regard the particle collides with a big body, and remove it from the computation. Also, when the heliocentric distance of a test particle gets larger than a certain value (hereafter we call it "elimination distance"), the particle's integration is stopped because it is we think too far. In most of previous researches, this elimination distance was set to 10 AU. We set the elimination distance to a larger value, 100 AU, which we think is better justified than 10 AU (see the discussion in section 3.1).

For the numerical integration scheme, we used the regularized MVS method (the source code called SWIFT_RMVS3) devised by Levison and Duncan (1994) based on the popular algorithm of Wisdom–Holman symplectic map (Wisdom and Holman, 1991). We have modified some routines of the SWIFT_RMVS3 code for our specific needs. To check the accuracy of our numerical integrations, in several cases we also used independent numerical schemes such as the Bulirsch-Stoer extrapolation method (Bulirsch and Stoer, 1966; Press et al., 1992) or the fourth-order time-symmetric Hermite integrator (Makino and Aarseth, 1992; Kokubo et al., 1998). The statistical results obtained by the regularized MVS overall agree with that by the extrapolation method or the Hermite scheme when we choose the stepsize of 4–8 days for SWIFT_RMVS3.

3. Numerical results

In this section we describe our numerical results regarding (i) removal rate, collisional probability, decay timescale of test particle population, and survivors, (ii) time sequence of collisions of particles, (iii) typical orbital evolution of some particles that hit planets, and (iv) the dynamics of survivors.

3.1 Collision probability, decay timescale

The lower part of Table 1 summarizes the collision probability of test particles on the planets and on the Sun for each of the simulations. As mentioned previously, the orbital integration for a test particle is stopped if it collides with the Sun or planets, or if its heliocentric distance exceeds 100 AU. For the initial conditions (1)(2)(3), approximately 70% of the particles collided with the Sun. The case (4) which is relatively far from the ν_6 resonance yields no collision on any planet, and only a small fraction of particles collide with the Sun. Table 1

About 10%–15% of the particles were removed by going too far away than 100 AU. According to our test integrations, this probability is slightly enhanced (+2% to +3%) when we used a smaller elimination distance, such as 10 AU that many other previous studies have used. Our test integration also indicates that when we use a larger elimination distance than 100 AU such as 1000 AU or 5000 AU, this probability is not significantly changed. If the orbit of a test particle is hyperbolic at a distance of O(1000AU), the particle is not likely to come back to the inner region again. And, even when the orbit of a test particle remains elliptic at the point of heliocentric distance of O(1000AU), the orbit of the particle is likely subsequently circularized by galactic tidal force. Then it is possible that the particle does not return to the inner planetary region for a very long time, a process that is part of the formation mechanism of the Oort cloud (cf. Duncan et al. 1987). Thus we consider our choice of 100 AU for the elimination distance to be dynamically better justified than the 10 AU of previous studies. It also allows us to obtain rough estimates of asteroid collision rates with the outer planets.

We included Mercury in our integrations in order to calculate the collision probability of test particles on the surface of this planet. No previous study has included Mercury, mainly because the incorporation of Mercury increases the computer time greatly, and also because the gravity of Mercury is considered so small that it might be safely ignored. To check the difference in collision probability with and without Mercury, we ran a set of numerical integrations starting from the same initial conditions as the case (2) without Mercury. The results of this run show that the collision probability of test particles on Venus in this run is about 4.5%, slightly less than the 5.06% when we included Mercury (Table 1, case (2)). The fraction of the solar colliders increased from 71.6% to 73.0% when we excluded Mercury. Collision probabilities for other planets are not very different with and without Mercury. This result suggests that Mercury has a small but possibly measurable effect on the collision probability on Venus, deflecting a fraction of sun-grazing objects that would otherwise collide with the Sun.

Figure 2 shows the decay rate of all the test particle populations for each of our initial conditions (1)–(7). The decay rate depends strongly on the location of disruption event, as well as on the initial ejection velocity, v_0. The decay rates for the initial conditions with $v_0 = 0.2$ km/s (1)(2)(3) look very similar, whereas that for the case (5) with $v_0 = 0.8$ km/s shows a much longer decay timescale, although a, e, I of the disruption center of the case (5) is same as those of the case (2). Generally, the smaller v_0 is, the stronger the dependence of the decay timescale on the initial disruption center. The decay timescales of the condition (6) and (7) are very different in spite of the fact that their v_0 is the same ($v_0 = 0.1$ km/s): (7) which is closer to the resonance center shows a shorter decay timescale, whereas (6) exhibits much longer decay timescale because the disruption center of (6) is further from the ν_6 resonance center. In particular, the very beginning part of the decay curve, up to ~ 5 Myr for the case (6) in Fig. 2 has a relatively shallow slope. This slow start owes to the slow diffusion of particles from the disruption center (6) to the ν_6 resonance center where their eccentricities and inclinations are quickly pumped up. We did not plot the decay curve for the initial condition (4) on Fig. 2 because only four particles were removed from this set over the entire 100 million year integration.

Fig. 2

3.2 Collision sequence

As in Table 1, several per cent of the asteroid fragments eventually hit the planets, mostly the terrestrial planets. Figures 3 and 4 show the histogram of the particles that collided with planets and the Sun, and the particles that went beyond 100 AU from the Sun for each of the datasets (1)–(7) except (4). Though both of Figs. 3 and 4 may look like typical examples of small number statistics, some systematic trends are notable: the peak of collision flux on planets comes first to Mars, then to the Earth, Venus, and finally to Mercury. The peak of the collisions to the Sun, as well as the peak of the particles that go too far away from the Sun, comes even earlier than the peak of the collisions to Mars. As we mention in the next section, the eccentricity and inclination of the particles that are close to the ν_6 resonance center are pumped up very quickly by the ν_6 itself and by the Kozai oscillation, in less than a few to ten Myr for the initial condition (1)(2)(3). Many of the particles whose eccentricities get very high directly hit the Sun, or encounter with Jupiter and get scattered outward, eventually eliminated from the system. This causes the rapid production/decay rate of the solar colliders and "too-far" particles. On the other hand, close encounters with the terrestrial planets reduce the semimajor axes of many particles, making them migrate toward the terrestrial planetary zone with a longer timescale. These particles are the candidates for planetary collisions.

Even when the asteroid fragments are widely scattered due to a large initial ejection velocity, such as the case (5) with $v_0 = 0.8$ km/s, the production and decay timescale of the solar colliders and the "too-far" particles is not so different from when the value of v_0 is smaller as in (1)(2)(3). This is because the initial orbital distribution of the fragments that belong to (5) overlaps the ν_6 resonance (Fig. 1), and some particles are very close to the resonance center from the beginning, which could lead to the rapid production rate of solar colliders and too-far particles. At the same time, the highly dispersed distribution of the particles of (5) provides a long tail in the flux of planetary colliders, as we see in the panels in the left columns of Fig. 4.

When the initial distribution of asteroid fragments is not so widely scattered (i.e. when their initial ejection velocity is small) but the location of the disruption event is away from the resonance center such as case (6), it takes much longer for particles to approach the resonance center. Hence the production and decay timescale of solar colliders, too-far particles, and planetary colliders get much longer (the middle panels of Fig. 4), compared with the cases of other initial conditions whose centers are closer to the ν_6 center. In contrast, when the initial ejection velocity of asteroid fragments is small and the location of disruption event is near the resonance center such as (7), the removal efficiency of asteroid fragments from the system is very high, and the decay timescale is very short as we see in the right panels of Fig. 4.

Fig. 3
Fig. 4

The results in Table 1 show that the integrated collision frequency for Venus over 100 million years is about 1.5 times larger than that for the Earth for all the initial conditions. Also, the collision probability for Mercury is about 1.2 to 3 times larger than that for Mars, except the case (6). Since our result shown in Table 1 is typical of small number statistics, the collision probability for each planet contains non-negligible uncertainties. For example, we got 11 collisions (0.56%) on Mercury and 18 collisions (0.91%) on Mars from the 1975 particles in case (6). But these numbers include the possible error of $11 \pm \sqrt{11} \sim 11 \pm 3.3$ and $18 \pm \sqrt{18} \sim 18 \pm 4.2$. Hence the conclusion that Mars has more collisions than Mercury in the case (6) might not hold

so obviously. This small number statistics problem underscores the need for the simulations using many more particles.

To take a closer look at the collision probability on planets, we took the case (2) as an example and recorded the number of particles that encountered with the Hill spheres of each terrestrial planet. Beginning with 2962 particles in the case (2), 55,202 encounters were detected at Mercury's Hill sphere. Also, 1,925,347 encounters with Venus' Hill sphere, 2,628,708 encounters with Earth's Hill sphere, and 871,638 encounters with Mars' Hill sphere were recorded during the 100 million year integration. These numbers of close encounters are large enough for us to statistically discuss the encounter probability. We calculated the root mean square of the encounter velocity $\langle v_{\rm e} \rangle$ of all the encounters at the surface of planetary Hill spheres, time-averaged over 100 million years. The time-averaged value of $v_{\rm e}$, $\langle v_{\rm e} \rangle$ are 34.7 km/s for Mercury, 25.8 km/s for Venus, 22.0 km/s for Earth, and 14.8 km/s for Mars. Since $\langle v_{\rm e} \rangle$ around each planetary Hill sphere is roughly equal to the Kepler velocity of test particles at encounter points, $\langle v_{\rm e} \rangle$ is the largest around Mercury's Hill sphere and the smallest around Mars' Hill sphere. We note that these values are larger than the escape velocity of each planet. Thus gravitational focusing is not significant, and the particle-in-a-box approximation gives relatively accurate estimates of collision probability. The proportions the $\langle v_{\rm e} \rangle$ values for Mercury, Venus, Earth, and Mars averaged over 100 million years and normalized by the value of the Earth is about $1.58 : 1.17 : 1 : 0.674$. The ratio of planetary surface area between these four planets normalized by the value of the Earth is about $0.146 : 0.900 : 1 : 0.283$. Simply multiplying these ratios gives us an approximate estimate of the relative collision probabilities of test particles on each planet, assuming the particle-in-a-box approximation. The resulting proportion $0.231 : 1.05 : 1 : 0.191$ is in reasonably good agreement with the collision probabilities in Table 1. This roughly explains why the collision frequency for Venus is slightly larger than that for the Earth and why that for Mercury is somewhat larger than that for Mars. The largest deviation from the particle-in-a-box approximation is seen for the collision probability of Venus to that of Earth; the particle-in-a-box approximation yields a ratio of 1.05 whereas the numerical simulations yield a ratio of 1.18–1.65 (Table 1).

Although the rough estimates that we described might be safely used for the qualitative explanation of the dynamical behavior of the asteroid fragments, it is also clear that we need many more particles to get much better statistics of direct planetary collisions, especially when we include the lunar orbit around the Earth. In particular, for the comparison between dynamical simulations and geological crater record, reliable collisional statistics produced from the direct integration of lunar orbit is necessary. Thus, for a future study we are preparing the direct integration of test particles including lunar orbital motion in our numerical models.

As for the the collision probabilities of test particles with the outer planets, they are generally low, which is also true in our numerical integrations. The strong gravitational field of large jovian planets, especially that of Jupiter and Saturn, mainly works for scattering particles, rather than letting them collide with the large planets. Because of this scattering effect, 10–15% of the fragments end up as "too-far" particles at the distance of 100 AU. In the actual solar system, some of those particles could be a potential source of the Oort cloud objects.

3.3 Typical orbital evolution of planetary colliders

Orbital evolution of near-Earth asteroids starting from resonance zones in the main belt is generally complicated and often chaotic (Gladman et al., 1997). In addition to the strong resonances such as ν_6 and other mean motion resonances, numerous number of weak resonances are effective to diffuse the orbits of asteroids until they get into the strong resonances (Morbidelli and Nesvorný, 1999). Here we describe a few dynamical characteristics of the particles that evolve toward the terrestrial planets in our numerical integrations. As the first stage, ν_6 itself is effective, and pumps up the eccentricity of nearby particles quite effectively. The timescale of the enhancement of eccentricities depends on the particle's distance from the resonance center, but typically less than one to a few million years under the initial conditions (1)(2)(3). Some of the particles collide with the Sun because of this quick enhancement of eccentricity, even before they experience many close encounters with planets. Once the eccentricity of particles around the resonance is enhanced to planetary-crossing values, close encounters between particles and planets occur, which change the semimajor axes of particles. When the semimajor axis of a particle is reduced, perihelia and aphelia of the particle go deeper inside the terrestrial planetary orbits. This can allow the collisions between planets and the particles. Since the planetary encounters get frequent first with Mars, then with Earth and the inner planets, the peak of planetary collisions comes to Mars first, then to the inner planets in order as seen in Figs. 3 and 4.

Fig. 5

Fig. 6

Figure 5 shows the typical orbital evolution of three planetary colliders starting from the initial condition (2). The panels (1[a–d]) in Fig. 5 are for a particle that hit the Earth, and the panels (2[a–d]) and (3[a–d]) are for two particles that collided with Venus. During the first one million years, the eccentricities of all three particles are pumped up rapidly due to the ν_6 resonance. Their orbits begin crossing the orbit of Mars within a million years followed by close encounters with the Earth, as shown by many abrupt changes in semimajor axis in the panel (1b) in Fig. 5. For the particle shown in the panels (1[a–d]) in Fig. 5, the combination of the eccentricity pump-up by the ν_6 resonance and the close encounters with Mars brought its perihelion near the Earth's orbit, and eventually caused the particle to hit the Earth. For the particles in the panels (2[a–d]) and (3[a–d]) in Fig. 5, planetary close encounters conveyed their perihelion distance near the orbit of Mercury with the timescale of a few million years, having the particles collide with Venus. The inclination of any particle does not show a significant change during their lifetimes (the panels [1–3]c).

The main outline of this three-stage mechanism, i.e. enhancement of eccentricity by $\nu_6 \rightarrow$ close encounters with planets $\rightarrow$ planetary collisions, has been obtained by Monte Carlo simulations already in the 1980's, and verified in numerical integrations in the 1990's (Wetherill, 1985; Farinella et al., 1994; Gladman et al., 1997; Morbidelli and Gladman, 1998). Our detailed numerical integrations can identify one more interesting dynamical feature here. In the orbital evolution of these particles, we can see the strong evidence of the Kozai mechanism (Kozai, 1962; Kinoshita and Nakai, 1991; Michel and Thomas, 1996). The Kozai mechanism (sometimes called the Kozai behavior, the Kozai oscillation, the Kozai state, the Kozai cycle, and the Kozai resonance), drives the eccentricity and the inclination of asteroids very high, such as $e \sim 1$ and $I \sim 90^\circ$ under certain conditions. In our integrations, certain number of particles exhibit the

Kozai behavior in a relatively short timescale such as a few to 10 million years when started from the initial locations (1)(2)(3). The Kozai behavior here is a production mechanism of some sun-grazers and solar colliders. The panels of (1[a–d]) and (2[a–d]) in Fig. 6 show typical Kozai behaviors seen in two of the particles started from the initial condition (2). These two particles experienced several planetary close encounters which changed their semimajor axis (1b and 2b) and eccentricity (1a and 2a) to the values that satisfy the condition of the Kozai mechanism in the later half of their dynamical lifetime. For these two particles, what we see is the circulation-type Kozai behavior; their arguments of perihelion circulate as in the panels (1c) and (2c), but they spend more time around $\omega = 0$ and $\omega = 180^\circ$ than at other values. The eccentricity of the two particles eventually reached near 1 with high inclinations, which led them to the collision to the Sun.

Interestingly, some particles survive the entire integration period (100 million years) even though they exhibit the Kozai behavior. The panels (3[a–d]) in Fig. 6 are the typical examples of the orbital elements of such a particle. This particle behaves quite differently from other particles shown in the panels (1[a–d]) and (2[a–d]) in Fig. 6. The argument of perihelion comes back and forth between circulation and libration, ending up with the libration around $\omega = 270^\circ$. This variation is again caused by the change of semimajor axis due to the close encounters with planets. The eccentricity and inclination of the particle was enhanced by this mechanism, but not enough for the particle to collide with the Sun. When this particle exhibits a typical libration-type Kozai behavior after time $t > 20$ Myr, the argument of perihelion always stays around $\omega = 270^\circ$ or 90°, keeping its inclination large ($I \sim 30$–60°). This possibly reduces the interaction with planets, providing a kind of protection mechanism for the particle from close encounters with planets. This protection mechanism is essentially the same as what Michel and Thomas (1996) demonstrated in the dynamical motion of some actual near-Earth asteroids.

As a possible projectile onto the Earth–Moon system, here we define an Earth-crossing object (hereafter we call ECO) as a particle whose perihelion distance q is smaller than the aphelion distance Q of the Earth, and whose aphelion distance is larger than the perihelion distance of the Earth (i.e. $q < Q_{\rm Earth}$ and $Q > q_{\rm Earth}$). This definition is approximately same as that of the combination of two NEA groups, Atens and Apollos; i.e. the ECOs compose a subset of NEAs. Examples of the time-dependent probability distribution of the orbital elements of the ECOs thus defined are shown in Figs. 7 and 8 for the initial conditions (3) and (6). In Fig. 7 for the initial condition (3), we can see the rapid enhancement of eccentricity in a few million years, as well as the gradual reduction of perihelion distance with the timescale of about 10 million years mainly because of the close encounters with planets, as described before. The Kozai behavior is clear in the panel of the argument of perihelion (bottom left). The density of particles are higher at around $\omega = 0$ and $\omega = 180^\circ$ in the first several million years, which demonstrates the existence of the circulation-type Kozai behavior. Figures 8 for the initial condition (6) shows qualitatively the same dynamical character (rapid enhancement of eccentricity, gradual reduction of perihelion distance, and the circulation-type Kozai behavior). But their timescale is much longer than in Figs. 7, because the initial location of the disruption event is away from the resonance center, and also because the particles of the initial condition (6) are concentrated in a smaller region than those of the initial condition (2) due to the smaller initial ejection velocity, $v_0 = 0.1$ km/s. The panel for the argument of perihelion in Figs. 8 (bottom left)

shows the libration-type Kozai behavior at around $\omega = 270^\circ$ in the later half of the integration period, which indicates that some particles survived over the whole integration period with this libration-type Kozai behavior, as exhibited in Fig. 6 (3c). Longitudes of ascending node of test particles are distributed uniformly in any integrations (bottom right panels).

Fig. 7

Fig. 8

3.4 Survivors

After 100 million year integrations, we still have many survivors (see the bottom of Table 1) that have not collided with planets or the Sun, or reached large heliocentric distances. Figure 9 shows the final orbital elements (semimajor axis, eccentricity and inclination) of the survivors starting from each of the initial conditions. These orbital elements are time-averaged over the final 5×10^5 years in order to obtain the values that are similar to their proper orbital elements. Most of the survivors have semimajor axes smaller than 2.5 AU. The particles that went well beyond the ν_6 resonance center from the initial locations were perturbed by other resonances, such as 3:1 or 2:1, and relatively quickly eliminated from the system by hitting the Sun or other planets, or ejected out of the system. The particles that are diffused to smaller semimajor axis have a long tail of survivors.

Almost all particles started from (4) have remained near their original positions where there is no strong resonance. Also, a large fraction of particles started from (5) and (6) are still confined in relatively limited areas in the orbital element space. In this sense, we may think that the particles started from (4)(5)(6) can form asteroid families, at least on timescales of 100 million years. However, long-term perturbations caused by numerous small resonances may diffuse this family-like structure, especially their proper eccentricities and inclinations, over longer periods such as 10^9 years. Initial conditions other than (4)(5)(6) do not yield a distinct asteroid family 100 million years after the disruption events, such as seen in Fig. 9 (1)(2)(3)(7). So, it would be difficult to find clear evidence of a very old disruption event, looking at the current orbital elements of family asteroids. In other words we cannot rule out the possible existence of many asteroid families in the distant past, because it is likely that they would be dispersed on 10^9 year timescale if they had been formed in the vicinity of a strong resonance area such as ν_6. This anticipation is supported by a recent estimate that more than 90% of the current asteroids may belong to families (Ivezić et al., 2002).

One feature that draws our attention in Fig. 9 is that many particles survive with high eccentricity and high inclination. For a closer look at this feature, we plot in Fig. 10 the inclination distribution of our near-Earth survivors from the cases (1)(2)(3) and (5) (the definition of the near-Earth survivors is the same as that of the ECOs in the section 3.3), other (non-near-Earth) survivors from the cases (1)(2)(3) and (5), currently known 1,413 ECOs out of 2,335 NEAs (Atens, Apollos, and Amors), and 234,230 main belt asteroids (MBAs) with the semimajor axis $2\text{AU} < a < 4\text{AU}$. We accumulated all the survivors for the cases (1)(2)(3) in Fig. 10 (b) and (e) because these three cases are not statistically very different in terms of the orbital elements of survivors.

Comparing the panel (a) for the currently known ECOs with (b) and (c) for our survivors, it is obvious that the inclination of the near-Earth survivors in our numerical integrations tends to be higher than the currently known ECOs (or NEAs). Also, comparing the panel (d) for the known MBAs with (e) for our survivors, we can see that non-near-Earth survivors that belong to the cases (1)(2)(3) also have higher-inclination distribution than the current MBAs. As we saw in the previous section, many of the long-term survivors exhibit the Kozai behavior that enhances their inclination to a great deal, which serves as a protection mechanism for the particles by reducing the frequency of close encounters with planets. This result suggests that the remnants

of old disruption events (more than 100 million years ago or older) are preferentially to be found amongst the high inclination ECOs or NEAs, or even among the high-inclination MBAs.

The inclination distribution of the non-near-Earth survivors from the case (5) tends to be in smaller inclination region (Fig. 10 (f)). This is because a large part of the main belt survivors for the case (5) still keep relatively smaller eccentricities and inclinations even after the 100 million year integration, as we saw in the panels (5) of Fig. 9. However, longer-term planetary perturbation and numerous weak resonances can push these survivors toward ν_6 that scatters them, eventually making their inclination distribution similar to that of the cases (1)(2)(3) as in Fig. 10 (e).

Fig. 9

Fig. 10

4. Discussion

In this section we discuss a few issues that might be significant in future development of this line of research: initial ejection velocity of asteroid fragments after the disruption event, the effect of the velocity dependence on fragment size, and the influence of the Yarkovsky thermal force.

The typical initial ejection velocity of asteroid fragments that we used in our numerical integrations, $v_0 = 0.1$ km/s or 0.2 km/s, is as large as the maximum estimation of what hydro- and N-body numerical simulations predict. Benz and Asphaug (1999) showed that the ejection velocities of order 0.1 km/s can be obtained for basaltic targets provided the impactor size is at least about half the parent body size when the impact velocity is 3–5 km/s which is the typical relative velocity in the current asteroid belt. Michel et al. (2001; see also Michel et al. 2002) numerically simulated a catastrophic disruption using an SPH and an N-body code in order to create an asteroid family with a small mass ratio between the largest fragments and the parent body, such as the Koronis family. Using the collision velocity of 3.25 km/s in their numerical experiment, the mean ejection speed of the particles greater than their numerical resolution (fragment diameter $D >$ 1–4 km) is 0.128 km/s with a root mean square of 0.088 km/s. If the random velocity of main belt asteroids was as large as the present one at the time of the disruption, the impact velocity between asteroids can be up to $\sim$ 5 km/s. In this sense the results of the numerical simulations such as Benz and Asphaug (1999) or Michel et al. (2001, 2002) are in favor of our assumption on v_0.

The results of some laboratory experiments have reported lower values of v_0, such as 0.001–0.01 km/s for the largest fragments (Fujiwara et al., 1989; Nakamura and Fujiwara, 1991; Martelli et al., 1994). However, the diameter range of the fragments that are produced from these laboratory experiments (such as $D < 10$ cm in Nakamura and Fujiwara (1991)) are much smaller than that of the actual asteroid fragments, as is the nature of laboratory experiments. In this size range, the high material strength might be able to keep the ejection velocity of fragments lower even if the collision velocity is high. Also, the result of the hydro-code simulation by Benz and Asphaug (1999) indicates that a high-mass and low-velocity projectile will lead to a higher fragment velocity than a high-velocity and a small-mass projectile because of the efficient momentum transfer of larger projectiles. Hence we believe that the value of v_0 that we use is no less reliable than a conjecture, if no more than a reasonable prediction.

Another thing that we have to be concerned is the assumption of equal-velocity disruption, i.e. every particle has the same v_0. In general, smaller fragments have higher ejection velocity than larger fragments, even when the equi-partition of kinetic energy is not fully realized. If we express the dependence of mean ejection velocity on fragment size by an index β as $v_0 \propto D^{-\beta}$, the SPH simulation by Michel et al. (2003) yields $\beta \sim 0.5$ for an impact on a pre-shattered target, and a smaller β for a monolithic target (Patrick Michel, private communication, 2003). Nakamura and Fujiwara (1991)'s laboratory experiments gives a similar value of β for basaltic targets. In addition, these experiments indicate that the distribution of v_0 of particular size fragments can have a significant scatter, such as 1–2 orders of magnitude, especially when the fragment size is small.

The dependence of v_0 on fragment size and its possible scatter can significantly extend the initial distribution of the asteroid fragments in orbital element space. For example, suppose the v_0 of a $D = 20$ km fragment is 0.2 km/s. Then, the fragments with $D = 0.1$ km have $v_0 \sim 2.8$ km/s when we assume the index value of $\beta = 0.5$. Since there are many more smaller fragments than larger fragments, v_0 of this large value enormously extends the distribution of particles on (e, a) or (I, a) plane. In Fig. 11 we plot an example of the initial distribution of test particles using the size-velocity dependence $v_0 \propto D^{-0.5}$, centered on the same location as that of the initial condition (2). We assumed that the maximum fragment has the diameter of about 16 km with the initial ejection velocity $v_0 = 0.2$ km/s. The smallest fragment would be $D = 0.4$ km with $v_0 = 1.26$ km/s. There are 6155 particles plotted in Fig. 11, as well as the particles that belong to the initial condition (2). While this extension of the orbital distribution of asteroid fragments might be another justification to use somewhat large initial ejection velocity for our numerical integration such as $v_0 = 0.8$ km/s, it can greatly delay the arrival of the asteroid fragments to the terrestrial planetary region, especially that of smaller fragments. Accordingly, the decay time of the asteroid flux can be very long, much longer than what our numerical integrations yield. Fig. 11

The choice of the initial ejection velocity is also influenced by the Yarkovsky effect. The Yarkovsky effect can deliver asteroids with $D < 20$ km from their parent bodies to resonance zones, which transport them to the terrestrial planetary orbits (Bottke et al., 2002b). This ability of the Yarkovsky effect can make asteroid families disperse over a long-time period, drifting the proper semimajor axes of the family asteroids inward and outward (Bottke et al., 2001). The estimates of the initial ejection velocity of currently existing asteroids (Zappalà et al., 1996; Cellino et al., 1999) are based on the assumption that the proper semimajor axis of the family asteroids are constant against long-term planetary perturbations (e.g., Milani et al. 1992). If the Yarkovsky effect can significantly spread the proper semimajor axes of family asteroids, the estimated value of v_0 using the current distribution of their proper semimajor axis might be too large.

Even if the small asteroid fragments are scattered very widely such as in Fig. 11 due to the velocity dependence on size, the capability of Yarkovsky effect to transport the asteroid fragments to resonance zones can effectively work, especially on smaller fragments. Hence, once a large number of fragments are produced around resonance zones, sooner or later they are likely to encounter with resonances and eventually be conveyed to the terrestrial planetary orbits. Thus both the wide spread of the asteroid distribution and the Yarkovsky effect can

work for a slow decay of the asteroid flux originated by a large disruption event not so close to a strong resonance zone in the main asteroid belt.

Our numerical model is still premature, not including the effects discussed in this section such as the Yarkovsky effect. Moreover, the number of particles that we have used is not enough to make a confident statistical statement in terms of the direct collision probability on the terrestrial planets, particularly for the Moon. The future direction of our research will be (i) to increase the number of test particles, (ii) to include the Moon in our numerical model, (iii) to take account of the size dependence of the initial velocities of asteroid fragments, and (iv) to incorporate the Yarkovsky effect in the integration scheme. Eventually we hope to obtain certain simulated crater records for the planets that can be compared directly with the observations of planetary surface.

5. Conclusions

We have explored the dynamical evolution of test particles with initial conditions near the ν_6 resonance in order to simulate the orbital evolution of fragments from a hypothetical asteroid break-up event. Compared with previous studies, our simulations follow an order of magnitude larger number of particles, and relax in many ways the simplifying assumptions of previous models. We calculated directly the collision probabilities on the Sun and each planet, and the dynamical lifetimes of asteroid fragments. We examined how these quantities depend upon the initial conditions (on both the distance of the break-up event from the ν_6 resonance and the velocity dispersion of the fragments). Our conclusions are summarized as follows (a–g):

(a) Decay timescale as function of initial conditions: The decay rate of the particle population starting from the vicinity of the ν_6 resonance depends on its location and the initial ejection velocity. If particles start from relatively closer locations to the resonance center with the initial ejection velocity $v_0 = 0.1$ or 0.2 km/s (such as the cases (1)(2)(3) or (7)), the half decay timescale is very short, less than ten million years. This result is consistent with the previous calculation by Gladman et al. (1997). When the initial location of particles are far from the resonance center (such as the case (6)), or when the ejection velocity v_0 is very large (such as the case (5)), the decay timescale becomes much longer, 50–60 million years or more.

(b) Implications for NEAs: In our numerical integrations, the orbital evolution of ECOs produced by a disruption in the main asteroid belt sometimes shows a very long tail such as in Fig. 8 for the case (6). The decay timescale of ECOs can be about 50 million years or more, depending on the initial location of disruption event. This timescale is much longer than what has previously estimated for NEAs or NEOs (cf. Gladman et al. 1997; Bottke et al. 2002a). Since the ECOs compose a subset of NEAs, this fact suggests that some fraction of the current observed NEAs could be a remnant of disruption events more than 50 million years ago or older. Also, since major part of the ECOs (or NEAs) in our numerical integrations have survived in high-inclination range through the Kozai behavior in our integrations. We cannot deny the possibility that some of the NEAs with high inclination are leftovers of old disruption events in the main asteroid belt.

(c) Implications for dispersion of ancient asteroid families: Our integrations first showed that after 100 million years integrations, some of the survived particles still form asteroid "families" (such as (4)(5)(6) in Fig. 9), but other particles do not show such family-like dynamical structure because of the long-term perturbations. It is possible that the family-like structures shown for (4)(5)(6) might disappear on billion year timescale. This implies that there could have been many asteroid families in the distant past that have already disappeared by now. Some of them could have formed with a larger initial ejection velocity than what we estimate from the currently existing asteroid families.

(d) Collision peak sequence: Our integrations showed the detailed collision peak sequence of asteroid fragments for terrestrial planets and the Sun. The peak of collision flux comes first to Mars, then to the Earth, Venus, and finally to Mercury. The timescale depends on the initial location of disruption and ejection velocity. The peak of the collisions to the Sun, as well as the peak of the particles that go too far away from the Sun, comes even earlier than the peak of the collisions to Mars. This is because many of the particles have their eccentricity enhanced very quickly due to the strong ν_6 resonance or the Kozai mechanism, which produces a lot of sun-grazing objects as well as Jupiter-encountering particles.

(e) Collision probabilities on Sun and on each planet: The relative collision probabilities on planets and on the Sun in our numerical integration are somewhat similar to the result by Gladman et al. (1997), especially in the cases close to the resonance center (such as (1)(2)(3)(7)): more than 70% of the particles hit the Sun, and more than 10% went too far from the Sun. The biggest difference between our and Gladman et al. (1997)'s result is that we observed more collisions on Venus than on the Earth (see Table 1) whereas Gladman et al. (1997)'s result indicates smaller collision probability on Venus. We believe that Venus could have slightly larger collision probability than the Earth due to the reason that we described in 3.2 (see also the point (f) below). The difference might also be ascribed to the fact that Gladman et al. (1997) used much fewer particles (~ 150) for their integrations, resulting in the small number statistics.

(f) Effect of Mercury: We included Mercury in our numerical integrations, which no previous studies did. According to our test integration without Mercury for comparison, the collision probability of test particles on Venus is about 4.5% without Mercury, slightly less than the 5.06% when we included Mercury (Table 1, case (2)). The fraction of the solar colliders increased from 71.6% to 73.0% when we excluded Mercury. This result suggests that Mercury has a small but possibly measurable effect on the collision probability of test particles on Venus, deflecting a part of sun-grazing objects that would otherwise collide with the Sun.

(g) Implications for the Oort cloud objects: In our numerical integrations, about 10%–15% of the particles were "removed" because their heliocentric distance exceeded 100 AU. This probability is slightly enhanced (+2% to +3%) when we used a smaller elimination distance such as 10 AU that many other previous studies have used. Our test integration also indicates that when we use a larger elimination distance than 100 AU such as 1000 AU or 5000 AU, this probability is not significantly changed. The particles that reached a distance of O(1000AU) probably do not return to the planetary region for a very long time largely because their orbits are likely circularized by galactic tidal force. This mechanism might have contributed to the addition of asteroid fragments to the Oort cloud. Since there could be many disruption events

near the resonance zones in the main asteroid belt, a significant number of asteroids might have migrated to the Oort cloud region through this mechanism, depending on the magnitude and the total number of such disruption events.

Acknowledgments

The authors have greatly benefited from stimulating discussions with and encouragement from David Kring and Robert Strom. Fumi Yoshida provided us some useful information on the observational fact of current asteroids. RM acknowledges research support from NASA grant NAG5–11661. Part of the numerical calculation was performed at Astronomical Data Analysis Computer Center, National Astronomical Observatory of Japan, Tokyo.

References

Benz, W., Asphaug, E., 1999. Catastrophic disruptions revisited. Icarus 142, 5–20.

Bottke, W.F., Vokrouhlický, D., Brož, M., Nesvorny, D., Morbidelli, A., 2001. Dynamical spreading of asteroid families by the Yarkovsky effect. Science 294, 1693–1696.

Bottke, W.F., Morbidelli, A., Jedicke, R., Petit, J.-M., Levison, H.F., Michel, P., Metcalfe, T.S., 2002a. Debiased orbital and absolute magnitude distribution of the near-Earth objects. Icarus 156, 399–433.

Bottke, W.F., Vokroulický, D., Rubincam, D.P., Brož, M., 2002b. The Effect of Yarkovsky Thermal Forces on the Dynamical Evolution of Asteroids and Meteoroids. In: Bottke, W.F., Cellino, A., Paolicchi, P., Binzel, R.P. (Eds.), Asteroid III, Univ. Arizona Press, Tucson, pp. 395–408.

Bulirsch, R., Stoer, J., 1966. Numerical treatment of ordinary differential equations by extrapolation methods. Num. Math. 8, 1–13.

Cellino, A., Michel, P., Tanga, P., Zappalà, V., 1999. The velocity and implications for the physics of catastrophic collisions. Icarus 141, 79–95.

Duncan, M., Quinn, T., Tremaine, S., 1987. The formation and extent of the solar system comet cloud. Astron. J. 94, 1330–1338.

Farinella, P., Froeschlé, Ch., Froeschlé, C., Gonczi, R., Hahn, G., Morbidelli, A., Valsecchi, G.B., 1994. Asteroid falling onto the Sun. nature, 371, 315.

Froeschlé, Ch., Morbidelli, A. (1994) The secular resonances in the solar system. In: Milani, A., Di Martino, M., Cellino, A. (Eds.), Proceeding of the 160th IAU Symposium, Asteroids, Comets, Meteors 1993, Kluwer Academic Publishers, Dordrecht, pp. 189–204.

Froeschlé, Ch., Hahn, G., Gonczi, R., Morbidelli, A., Farinella, P., 1995. Secular resonance and the dynamics of Mars-crossing and near-Earth asteroids. Icarus 117, 45–61.

Fujiwara, A., Cerroni, P., Davis, D.R., Di Martino, M., Holsapple, K., Housen, K., Ryan, E.V., 1989. Experiments and scaling laws for catastrophic collisions. In: Binzel, R.P., Gehrels, T., Matthews, M. (Eds.), Asteroid II, Univ. Arizona Press, Tucson, pp. 240–265.

Gladman, B., Migliorini, F., Morbidelli, A., Zappalà, V., Michel, P., Cellino, A., Froeschlé, C., Levison, H.F., Bailey, M., Duncan, M., 1997. Dynamical lifetimes of objects injected into asteroid belt resonances. Science 277, 197–201.

Ivezić, Ž., Lupton, R.H., Juric, M., Tabachnik, S., Quinn, T., Gunn, J.E., Knapp, G.R., Rockosi, C.M., Brinkmann, J., 2002. Color confirmation of asteroid families. Astron. J. 124, 2943–2948.

Kinoshita, H., Nakai, H., 1991. Secular perturbations of fictitious satellites of Uranus. Celes. Mech. Dyn. Astron. 52, 293–303.

Kokubo, E., Yoshinaga, K., Makino, J., 1998. On a time-symmetric Hermite integrator for planetary N-body simulation. Mon. Not. R. Astron. Soc. 297, 1067–1072.

Kozai, Y., 1962. Secular perturbations of asteroids with high inclination and eccentricity. Astron. J. 67, 591–598.

Levison, H.F., Duncan, M.J., 1994. The long-term dynamical behavior of short-period comets. Icarus 108, 18–36.

Makino, J., Aarseth, S.J., 1992. On a Hermite integrator with Ahmad-Cohen scheme for gravitational many-body problems. Publ. Astron. Soc. Japan 44, 141–151.

Martelli, G., Ryan, E.V., Nakamura, A.M., Giblin, I., 1994. Catastrophic disruption experiments: recent results. Planet. Space Sci. 42, 1013–1026.

Michel, P., Thomas, F., 1996. The Kozai resonance for near-Earth asteroids with semimajor axis smaller than 2 AU. Astron. Astrophys. 307, 310–318.

Michel, P., Benz, W., Tanga, P., Richardson, D.C., 2001. Collisions and gravitational reaccumulation: Forming asteroid families and satellites. Science 294, 1696–1700.

Michel, P., Benz, W., Tanga, P., Richardson, D.C., 2002. Formation of asteroid families by catastrophic disruption: simulations with fragmentation and gravitational reaccumulation. Icarus 160, 10–23.

Michel, P., Benz, W., Richardson, D.C., 2003. Disruption of fragmented parent bodies as the origin of asteroid families. nature 421, 608–611.

Milani, A., Knežević, Z., 1992. Asteroid proper elements and secular resonances. Icarus 98, 211–232.

Morbidelli, A., Gladman, B., 1998. Orbital and temporal distribution of meteorites originating in the asteroid belt. Meteor. Planet Sci. 33, 999–1016.

Morbidelli, A., Henrard, J., 1991. Secular resonances in the asteroid belts: theoretical perturbation approach and the problem of their location. Celes. Mech. Dyn. Astron. 51, 131–167.

Morbidelli, A., Nesvorný, D., 1999. Numerous weak resonances drive asteroids toward terrestrial planets orbits. Icarus 139, 295–308.

Nakamura, A., Fujiwara, A., 1991. Velocity distribution of fragments formed in a simulated collisional disruption. Icarus 92, 132–146.

Press, W.H., Teukolsky, S.A., Vetterling, W.T., Flannery, B.P., 1992. Numerical Recipes in Fortran (2nd edition), Cambridge University Press, Cambridge, UK.

Wetherill, G.W., 1979. Steady state populations of Apollo-Amor objects. Icarus 37, 96–112.

Wetherill, G.W., 1985. Asteroidal source of ordinary chondrites. Meteoritics 20, 1–22.

Wetherill, G.W., 1987. Dynamical relations between asteroids, meteorites and Apollo–Amor objects. R. Soc. London Philos. Trans. 323, 323–337.

Wetherill, G.W., 1988. Where do the Apollo objects come from?. Icarus 76, 1–18.

Wisdom, J., 1983. Chaotic behavior and the origin of the 3/1 Kirkwood gap. Icarus 56, 51–74.

Wisdom, J., Holman, M., 1991. Symplectic maps for the N-body problem. Astron. J. 102, 1528–1538.

Zappalà, V., Cellino, A., Dell'oro, A., Migliorini, F., Paolicchi, P., 1996. Reconstructing the original ejection velocity fields of asteroid families. Icarus 124, 156–180.

Zappalà, V., Cellino, A., Gladman, B., Manley, S., Migliorini, F., 1998. Asteroid showers on Earth after family breakup events. Icarus 134, 176–179.

Case	(1)	(2)	(3)	(4)	(5)	(6)	(7)
a (AU)	2.05	2.05	2.05	2.3	2.05	2.15	2.08
e	0.05	0.10	0.20	0.25	0.10	0.10	0.15
I (deg)	1.43	2.87	5.73	24.0	2.87	2.87	4.30
ω (deg)	330.1	181.3	206.5	310.5	311.3	81.3	35.9
Ω (deg)	149.8	103.7	192.7	37.3	114.7	121.0	103.7
l (deg)	55.5	102.6	56.0	155.4	97.9	205.4	66.5
v_0 (km/s)	0.2	0.2	0.2	0.2	0.8	0.1	0.1
N	1973	2962	1978	1000	2173	1975	1972
Sun (%)	66.3	71.6	70.0	0.40	45.7	51.9	74.7
Mercury (%)	0.71	0.68	1.11	0	1.06	0.56	0.91
Venus (%)	6.18	5.06	5.16	0	3.41	3.19	5.17
Earth (%)	4.21	3.17	3.49	0	2.90	2.38	3.14
Mars (%)	0.51	0.64	0.76	0	0.92	0.91	0.30
Jupiter (%)	1.01	0.57	0.30	0	0.46	0.10	0.61
Saturn (%)	0.05	0.03	0.05	0	0	0	0.05
Uranus (%)	0	0	0	0	0	0	0
Neptune (%)	0	0	0	0	0	0	0
$>$ 100AU (%)	14.2	13.0	11.8	0	9.62	11.3	12.8
survivors (%)	5.47	4.02	6.22	99.6	34.7	28.5	0.96

Table 1: Osculating orbital elements of the locations of each disruption center in our numerical integrations, ejection velocity v_0, the number of test particles N, and the collision probability (%) of test particles that hit the planets and the Sun or went beyond 100 AU over 100 million years, as well as the probability of survivors.

Figure captions

Figure 1. Initial osculating orbital elements of the asteroid fragments in our numerical integrations. (a) Eccentricity e and semimajor axis a. (b) Inclination I and semimajor axis a. Approximate location of the secular resonance ν_6 is shown by dashed lines in each panel (cf. Morbidelli and Henrard, 1991).

Figure 2. Relative fraction of active (survived) test particles started from each of the initial conditions (1)(2)(3)(5)(6)(7).

Figure 3. The number of particles that collided with the terrestrial planets and the Sun, and that went beyond 100 AU over 100 million years starting from the initial conditions (1; left panels), (2; middle panels) and (3; right panels).

Figure 4. Same as Fig. 3, but for the initial conditions (5; left panels), (6; middle panels), and (7; right panels).

Figure 5. Examples of the typical evolution of the orbital elements (osculating eccentricity, semimajor axis, inclination, perihelion distance) of three particles from the case (2). The first particle in the panels (1[a–d]) hit the Earth, and the other two particles in (2[a–d]) and (3[a–d]) hit Venus.

Figure 6. More examples of the typical evolution of the orbital elements (osculating eccentricity, semimajor axis, inclination, argument of perihelion) of three particles from the case (2). The first two particle in the panels (1[a–d]) and (2[a–d]) collided with the Sun, and the third particle in (3[a–d]) survived over the 100 million year integration.

Figure 7. Time-dependent orbital distribution of ECOs of the initial condition (3) over 50 million years. (Top left) Semimajor axis. (Top right) Eccentricity. (Middle left) Perihelion distance. (Middle right) Inclination. (Bottom left) Argument of perihelion. (Bottom right) Longitude of ascending node. The maximum probability density (= average number of ECOs) is different from panel to panel.

Figure 8. Same as Fig. 7, but for the particles that belong to the initial condition (6) over 100 million years.

Figure 9. Final semimajor axis, eccentricity, and inclination of the particles that survived 100 million years for each initial condition. All elements are averaged over final 5×10^5 years.

Figure 10. Distribution of the inclination of the survivors of the cases (1)(2)(3) and (5), currently known ECOs, and main belt asteroids. (a) 1,413 ECOs out of 2,335 NEAs (Atens, Apollos, and Amors), (b) near-Earth survivors from our (1)+(2)+(3), (c) near-Earth survivors from our (5), (d) 234,230 MBAs with semimajor axis 2AU $< a <$ 4AU, (e) other (non-near-Earth) survivors from our (1)+(2)+(3), and (f) other survivors from our (5).

Figure 11. An example of the initial distribution of 6155 test particles using the size-velocity dependence $v_0 \propto D^{-0.5}$. (a) Osculating eccentricity and semimajor axis. (b) Osculating inclination and semimajor axis. The initial distribution of the particles of the initial condition (2) is

also plotted as a reference, concentrated around the point of $a = 2.05$AU, $e = 0.1$, and $I = 2.87$ degree.

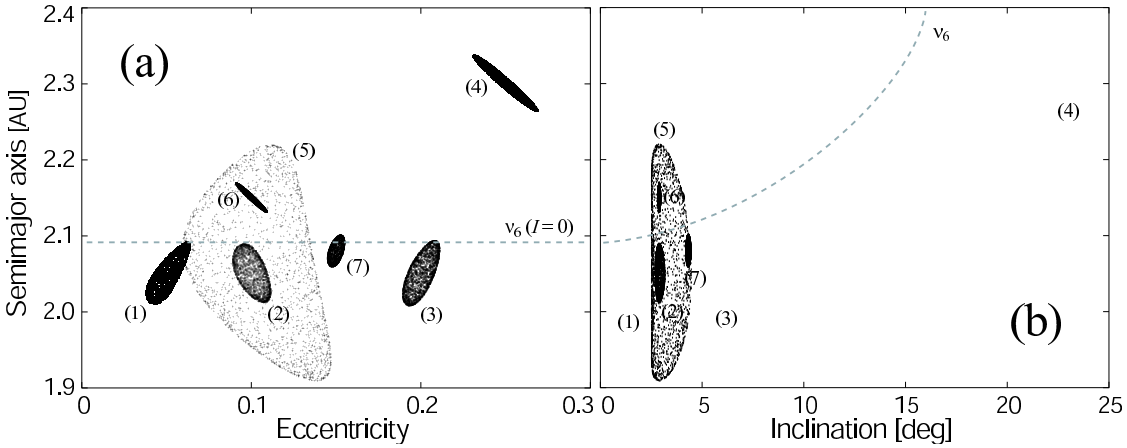

Figure 1: Ito and Malhotra

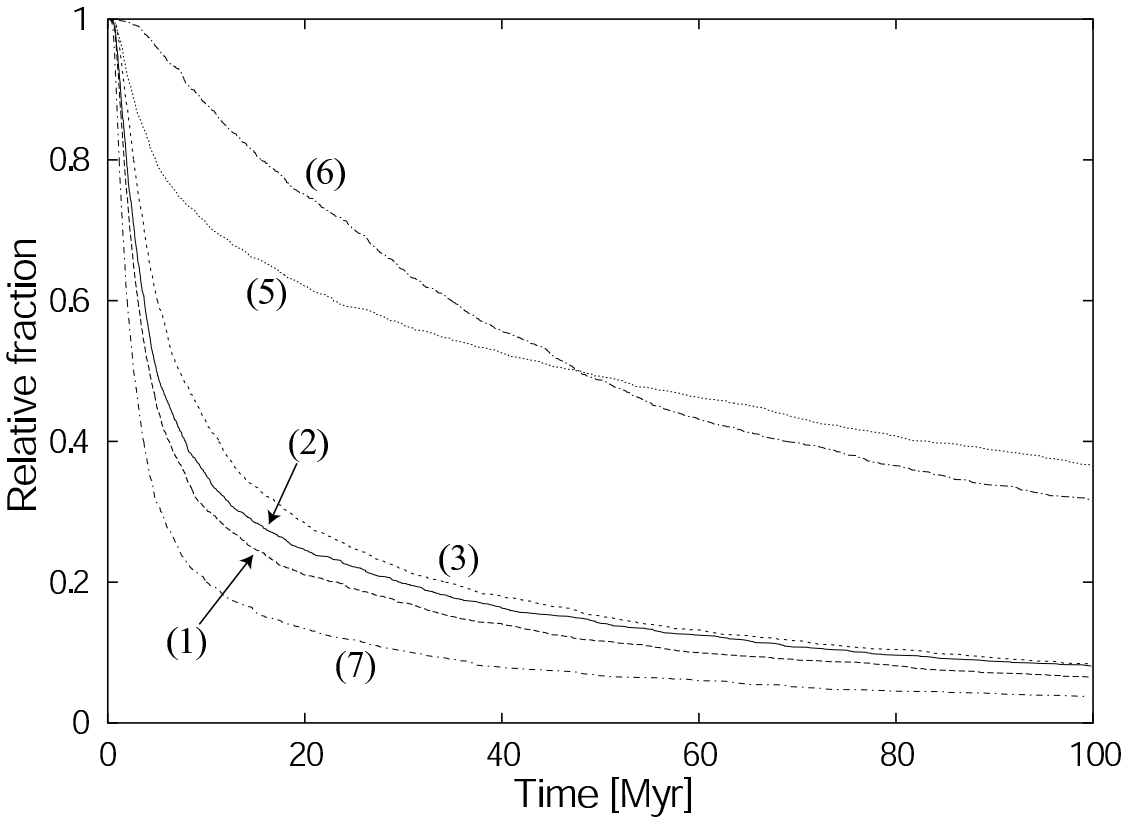

Figure 2: Ito and Malhotra

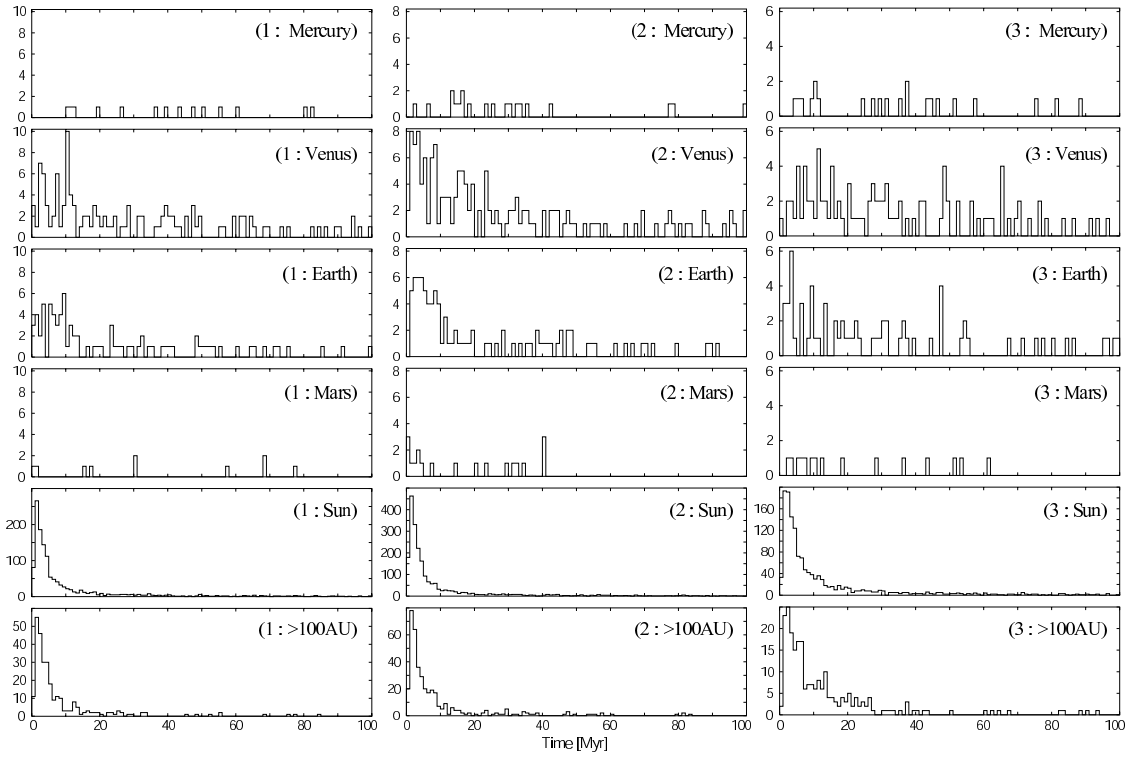

Figure 3: Ito and Malhotra

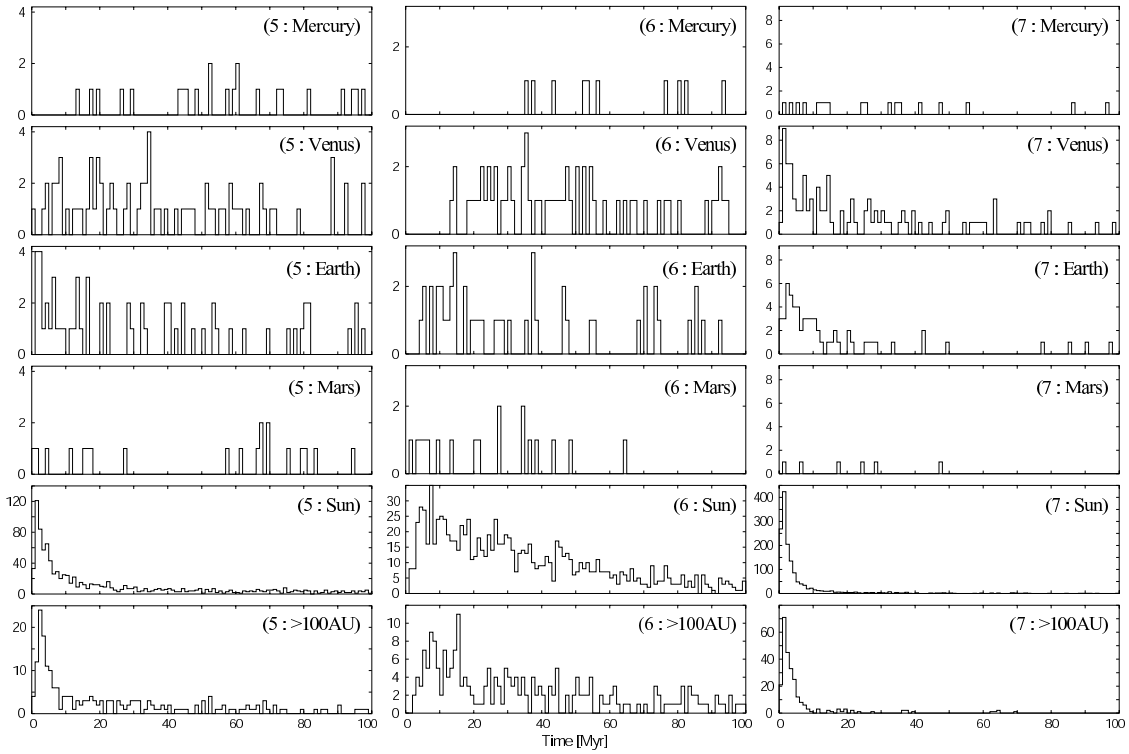

Figure 4: Ito and Malhotra

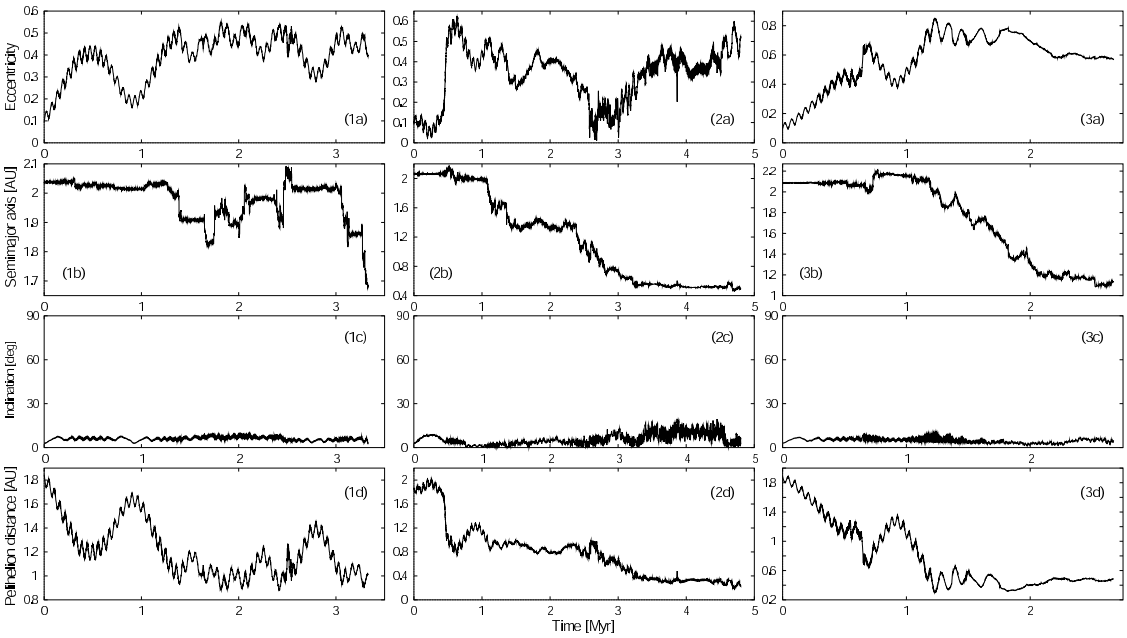

Figure 5: Ito and Malhotra

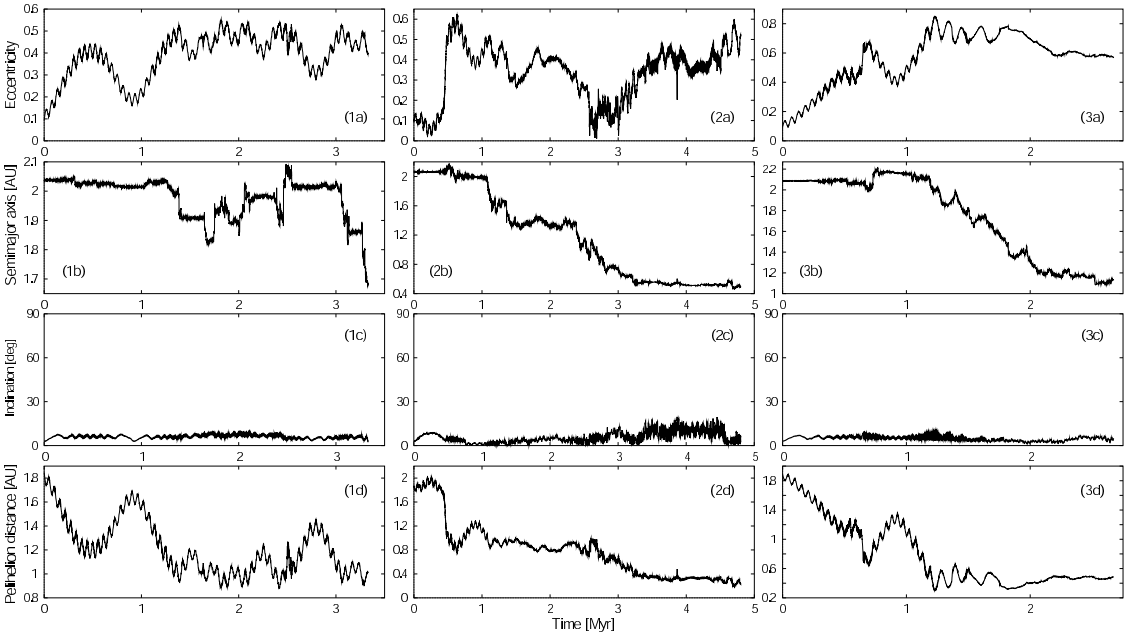

Figure 6: Ito and Malhotra

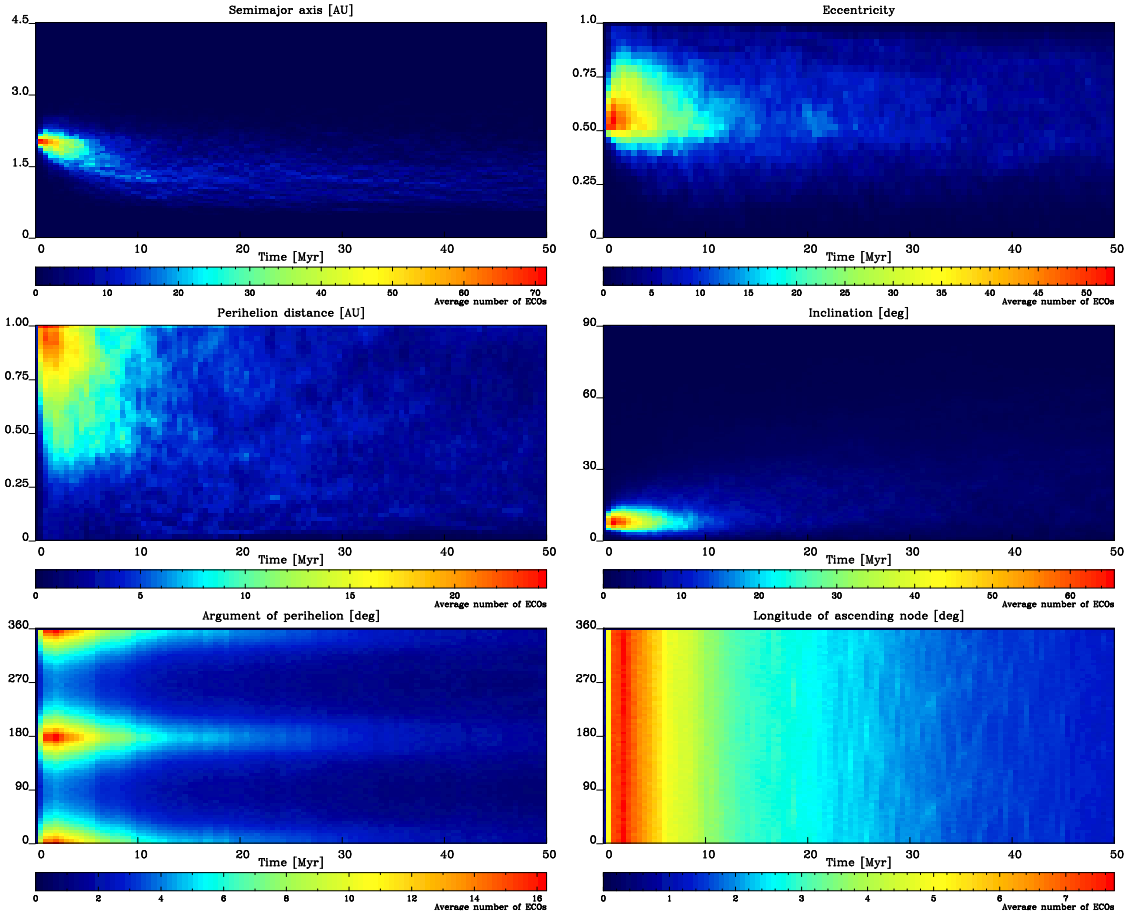

Figure 7: Ito and Malhotra

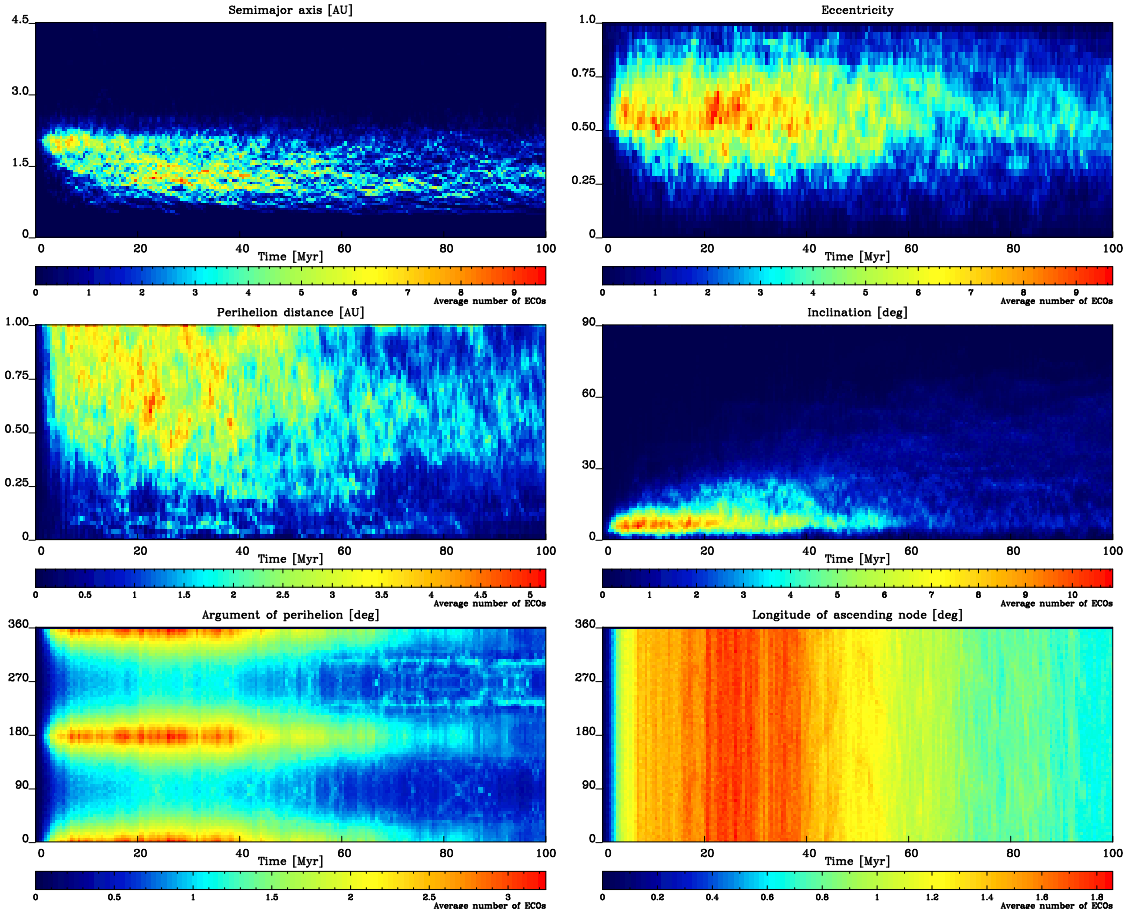

Figure 8: Ito and Malhotra

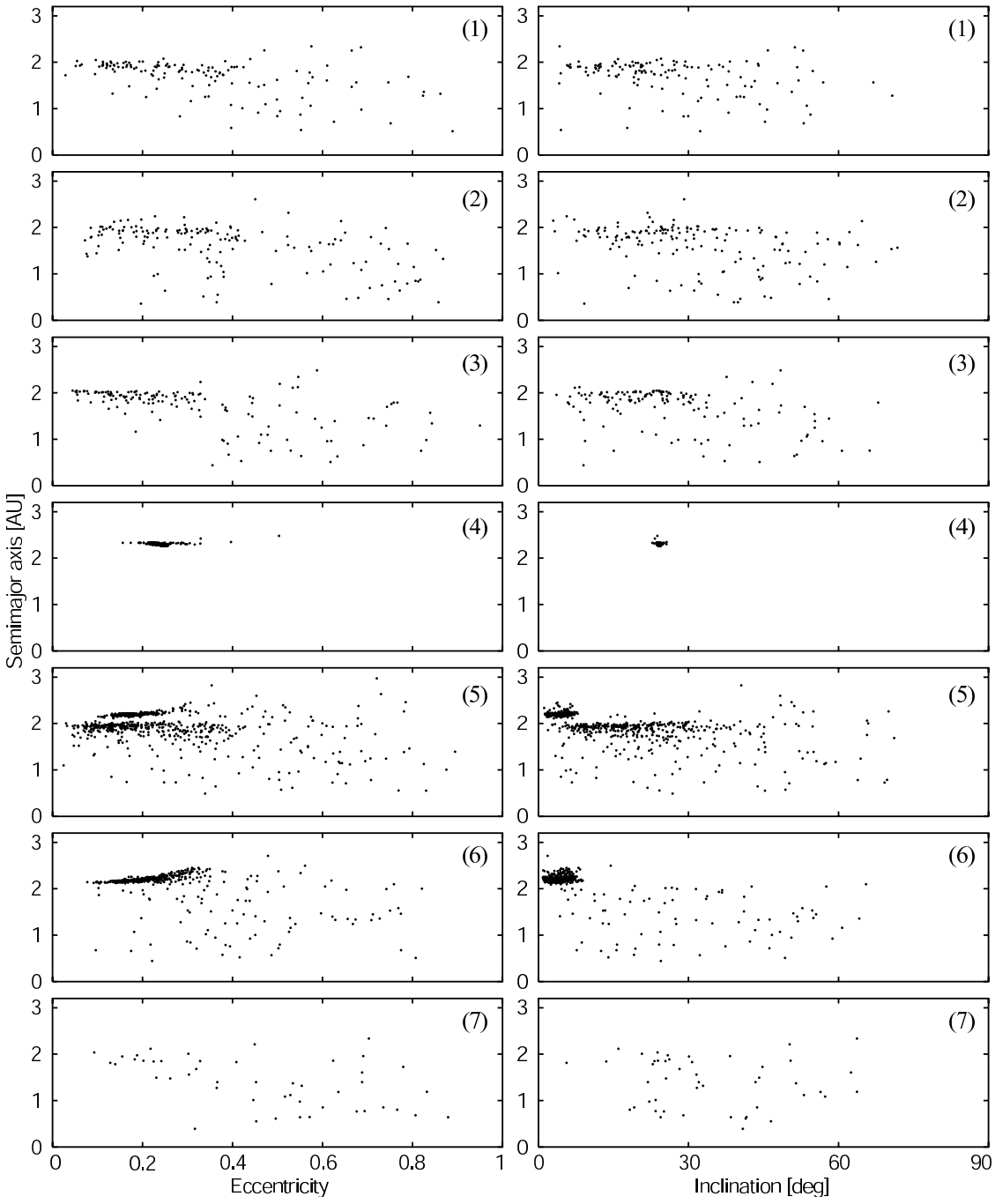

Figure 9: Ito and Malhotra

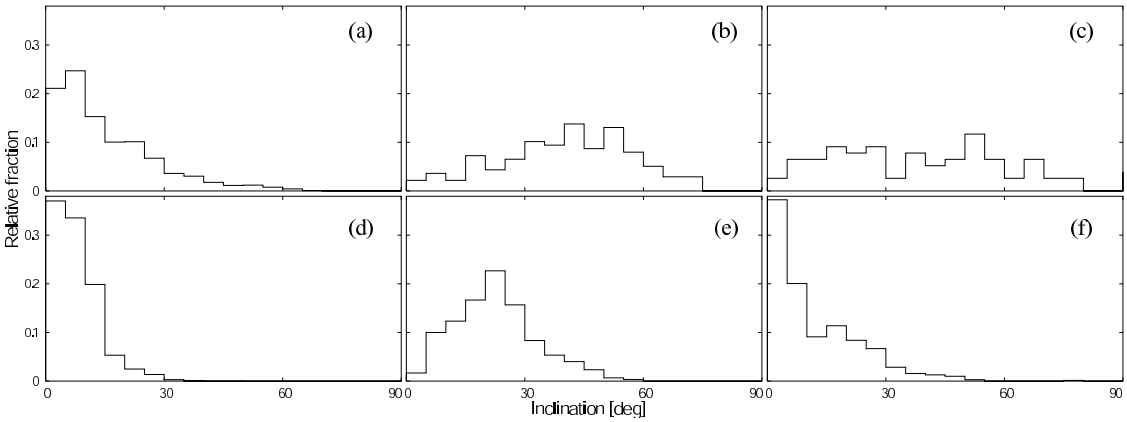

Figure 10: Ito and Malhotra

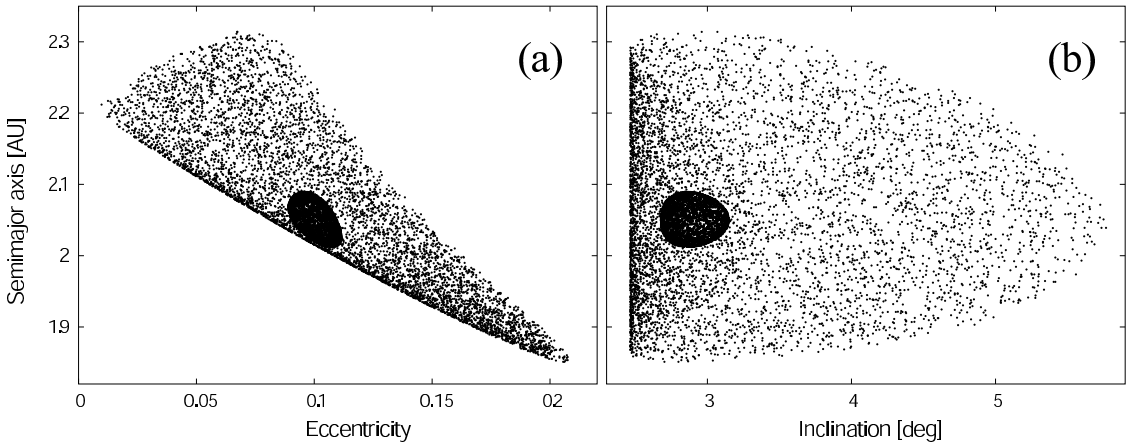

Figure 11: Ito and Malhotra